Spacecraft Observations and Theoretical Understanding of Slow Electron Holes

Sergey R. Kamaletdinov*
Space Research Institute, Moscow 117997, Russia and
Department of Physics, Moscow State University, Moscow 119234, Russia

Ian H. Hutchinson
Plasma Science and Fusion Center, Massachusetts Institute of Technology, Cambridge, Massachusetts 02139, USA

Ivan Y. Vasko
Space Sciences Laboratory, University of California at Berkeley, Berkeley, California 94720, USA
and Space Research Institute of Russian Academy of Sciences, Moscow 117997, Russia

Anton V. Artemyev
University of California, Los Angeles, Los Angeles, California 90095, USA
and Space Research Institute of Russian Academy of Sciences, Moscow 117997, Russia

Ajay Lotekar
Swedish Institute of Space Physics, Uppsala 752 37, Sweden

Forrest Mozer
Space Sciences Laboratory, University of California at Berkeley, Berkeley, California 94720, USA
and Department of Physics, University of California at Berkeley, Berkeley, California 94720, USA

(Received 8 May 2021; revised 15 August 2021; accepted 7 September 2021; published 15 October 2021)

We present Magnetospheric Multiscale observations showing large numbers of slow electron holes with speeds clustered near the local minimum of double-humped velocity distribution functions of background ions. Theoretical computations show that slow electron holes can avoid the acceleration that otherwise prevents their remaining slow only under these same circumstances. Although the origin of the slow electron holes is still elusive, the agreement between observation and theory about the conditions for their existence is remarkable.

DOI: 10.1103/PhysRevLett.127.165101

Multisatellite space observations of electron holes, Debye-scale electrostatic solitary waves of Bernstein-Green-Kruskal type [1–5], have firmly established that these structures can have speeds comparable to local ion thermal velocity [6–10]. This is actually surprising, because theory and simulations indicate that the interaction of such slow electron holes with ions normally prevents their speeds remaining at or below the ion thermal velocity [11–13]. The close attention to these nonlinear structures, which are observed in reconnection current sheets [6,7], plasma sheet [8,9], and collisionless shocks [10,14,15], arises in part because they might cause electron acceleration [16–19] and anomalous plasma resistivity [20–24]. Although the origin of these structures in space plasma is still elusive, in this Letter we resolve the problem of existence of slow electron holes. We show experimentally that slow electron holes move at speeds near the local minimum of a double-humped background ion velocity distribution, and this is just what is required, according to recent theory [25], to prevent the self-acceleration observed in simulations. This is a remarkable example of how the properties of Debye-scale structures are controlled by the kinetic features of the ion distribution function.

The experimental results are based on analysis of slow electron holes observed aboard four Magnetospheric Multiscale (MMS) spacecraft [26] in a particular interval in the Earth's plasma sheet. Importantly, the presented interval is not exceptional. The results are supported by a statistical analysis of slow electron holes collected in several other intervals in the Earth's plasma sheet (see Supplemental Material [27], which includes Ref. [28]).

Figure 1 presents MMS1 measurements over about a 3 min interval on August 4, 2017, when the MMS spacecraft were located at about 20 Earth radii from the Earth in the plasma sheet. Panels (a)–(c) show that the magnetic field of about 30 nT was relatively stable and directed toward the Earth, the plasma density was around 1.25 cm^{-3}, and the ion flow velocity stayed within 200 km/s. The electron and ion temperatures were, respectively, around 500 eV and 5 keV, though the ion velocity

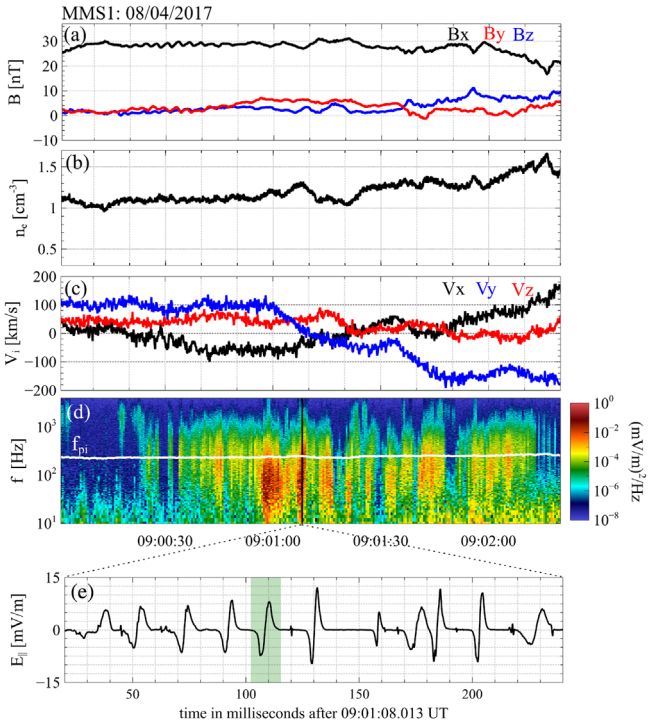

FIG. 1. Magnetospheric Multiscale observations in the Earth's plasma sheet on August 4, 2017 around 09:00:00 UT. We present measurements of MMS1, while other MMS spacecraft, being located within 10 kilometers of MMS1, provide identical overviews. Panels (a)–(c) present three components of the magnetic field measured at 128 samples/s by the flux gate magnetometer [29], electron density available at 30 ms cadence, and three ion bulk velocity components available at 150 ms cadence. The electron and ion parameters are moments of electron and ion velocity distribution functions measured at respectively 30 and 150 ms cadence by the fast plasma investigation instrument [30]. The magnetic field and ion bulk velocities are presented in the geocentric solar ecliptic (GSE) coordinate system with the x axis toward the Earth, the z axis perpendicular to the ecliptic plane and the y axis completing the right-hand coordinate system. Panel (d) presents the fast Fourier transform spectrum of the parallel electric field $E_\parallel$ measured at 8192 samples/s resolution by the axial and spin-plane double probes [31,32]. The local proton plasma frequency f_{pi} is indicated in the spectrum. Panel (e) presents a close view of the parallel electric field waveform over about 200 ms. The analysis of the highlighted solitary wave is presented in Fig. 2.

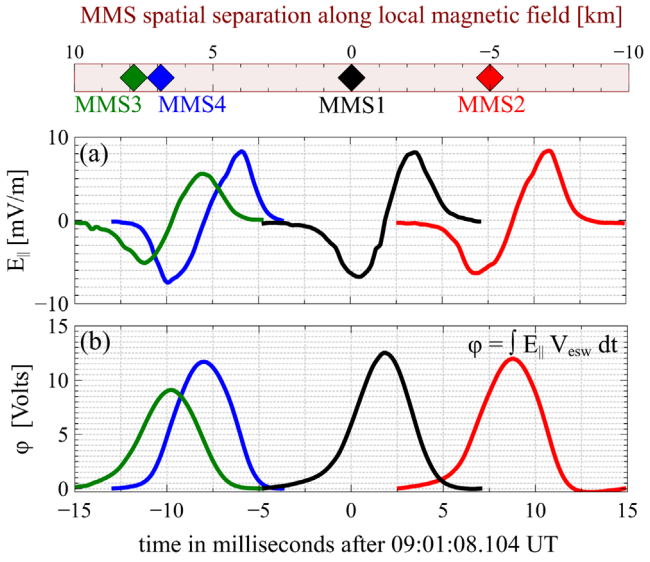

FIG. 2. Multisatellite analysis of the solitary wave (highlighted in Fig. 1) observed sequentially on four MMS spacecraft. Panel (a) presents parallel electric field $E_\parallel$ measured aboard each MMS spacecraft. The spatial separations between MMS spacecraft along the local magnetic field are presented above panel (a). The spatial separations between MMS spacecraft in the plane perpendicular to the local magnetic field were within 10 km (not shown). The time delay between observations of the solitary wave on a pair of spacecraft and the known distance between that pair of spacecraft along the magnetic field allow estimating the solitary wave velocity in the spacecraft frame by the two-spacecraft interferometry. The three velocity estimates corresponding to MMS1-MMS2, MMS1-MMS3, and MMS1-MMS4 are −760, −695, and −705 km/s; the averaged velocity value is $V_{\rm esw} \approx -720$ km/s. The negative velocity indicates propagation antiparallel to the local magnetic field. Panel (b) presents electrostatic potentials corresponding to $E_\parallel$ observed aboard each MMS spacecraft, which were computed as $\varphi = \int E_\parallel V_{\rm esw} dt$.

distribution function was not Maxwellian (see below). Note that ions were essentially protons, because densities of oxygen and helium ions were negligible, less than 1% of the plasma density. The spectrum of parallel electric field fluctuations in panel (d) shows the presence of broadband wave power between about 10 Hz and 1 kHz, around the local proton plasma frequency, $f_{pi} \approx 250$ Hz. The electric field waveforms measured continuously at 8192 samples/s resolution showed that the broadband wave power corresponds to electrostatic solitary waves with bipolar parallel electric fields. The waveform of the parallel electric field $E_\parallel$ in panel (e) exemplifies solitary waves observed over the entire interval. The perpendicular electric fields of the solitary waves were about ten times smaller than parallel electric field amplitudes (not shown). Using the previously described methodology [9], in this interval we collected 750 solitary waves observed sequentially on four MMS spacecraft.

Figure 2 presents one of the solitary waves observed on four MMS spacecraft in order of MMS3-MMS4-MMS1-MMS2. According to spatial separations between MMS spacecraft, this order is consistent with propagation antiparallel to the local magnetic field. Using the spatial separation between a pair of MMS spacecraft along the magnetic field, we can estimate the solitary wave speed in the spacecraft frame by the two-spacecraft interferometry. The speed estimates obtained by the interferometry between MMS1 and other MMS spacecraft are 760, 695, and 705 km/s. The consistency of the different velocity

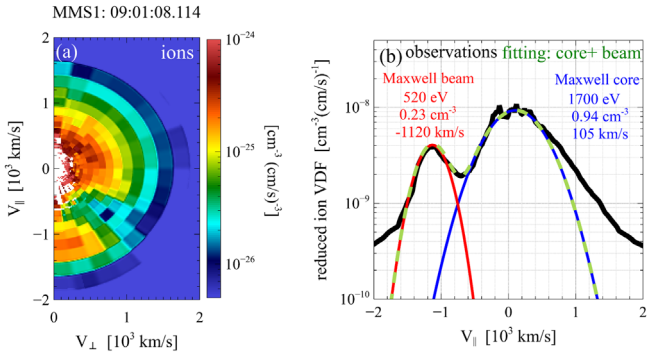

FIG. 3. The ion velocity distribution functions (VDF) measured at 150 ms cadence aboard MMS1 around the moment closest to the occurrence of the solitary wave shown in Fig. 2. Panel (a) presents the ion VDF in dependence on velocities parallel and perpendicular to the local magnetic field, while panel (b) presents reduced ion VDF computed as $\int \mathrm{VDF}(V_\parallel, V_\perp) 2\pi V_\perp dV_\perp$. The reduced ion VDF is fitted to a combination of beam and core populations described by drifting Maxwell distributions. The best fit models and the best fit parameters (density, drift velocity, and temperature) are presented in panel (b).

estimates is a strong indication that various MMS spacecraft indeed observe the same solitary wave. On a timescale of about 20 ms that it takes to propagate from MMS3 to MMS2, the solitary wave speed deviates from its averaged value of 720 km/s by less than a few percent. This is a strong indication of stable solitary wave propagation on a timescale of at least a few inverse of f_{pi}. The knowledge of the solitary wave speed allows translating the peak-to-peak temporal width of $E_\parallel$ into spatial width of about 3 km that is about 20 Debye lengths. Panel (b) presents the electrostatic potentials corresponding to $E_\parallel$ observed aboard each MMS spacecraft, $\varphi = \int E_\parallel V_{\mathrm{esw}} dt$, where $V_{\mathrm{esw}} = -720$ km/s is the averaged velocity of the solitary wave. The solitary wave is of positive polarity with amplitude of about 10 V that is a few percent of the local electron temperature. Note that the speed of the solitary wave in the plasma frame is not very different from the speed in the spacecraft frame, because ion flow velocity parallel to the local magnetic field was around −10 km/s [Fig. 1(c)].

The results of similar interferometry analysis for all 750 solitary waves are summarized below (see Supplemental Material [27] for details). The solitary waves are of positive polarity with amplitudes below 0.1 of local electron temperature and spatial widths from a few to a few tens of Debye lengths. Positive correlation observed between the amplitudes and spatial scales of the solitary waves is consistent with electron holes [5] and opposite to expectations for ion-acoustic solitons [33]. In both spacecraft and plasma frame, the solitary waves have velocities around −700 km/s that is on the order of the ion thermal velocity and around a few percent of the electron thermal velocity. Based on the revealed properties, we interpret the solitary waves in terms of slow electron holes.

Figure 3 presents ion velocity distribution function (VDF) observed aboard MMS1 around the moment closest to observations of the solitary wave in Fig. 2.

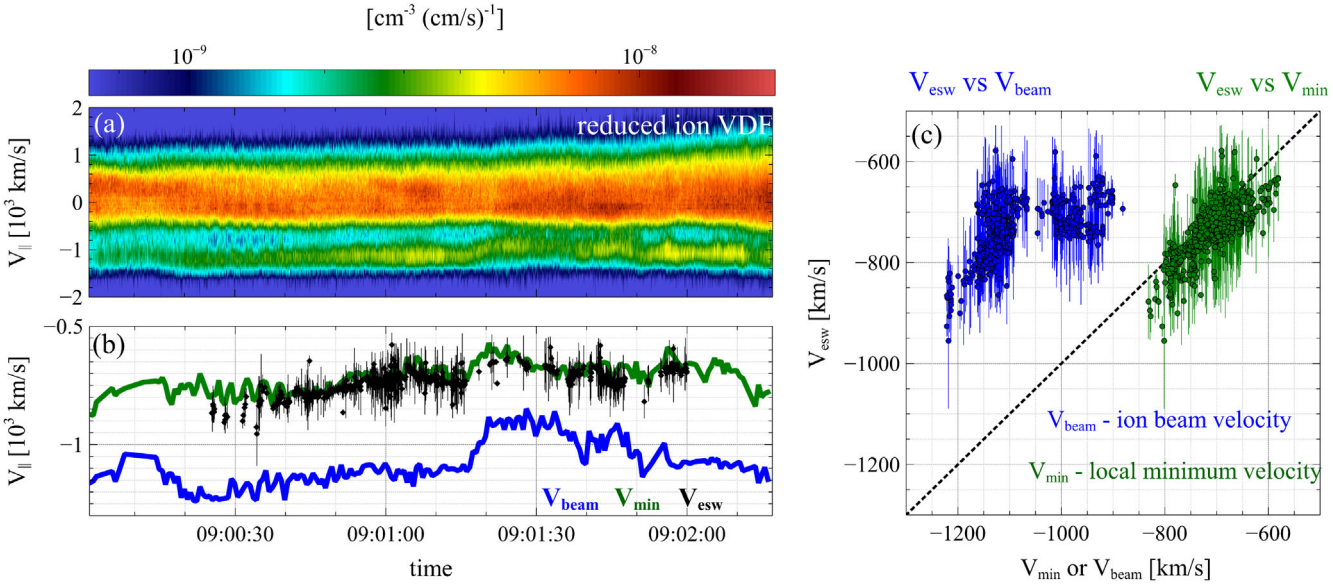

FIG. 4. Panel (a) presents the reduced ion velocity distribution function at 150 ms cadence computed using ion distribution functions measured aboard MMS1. Panel (b) presents velocities V_{beam} and V_{min} corresponding respectively to the local maximum (ion beam) and local minimum of the reduced ion VDF. Superimposed in panel (b) are velocities V_{esw} of all 750 solitary waves observed on four MMS spacecraft in the considered interval. Panel (c) presents the analysis of potential correlations of V_{beam} versus V_{esw} and V_{min} versus V_{esw}. All the velocities are in the spacecraft frame. The errors bars of V_{esw} in panels (b) and (c) are determined by minimum and maximum values among the three velocity estimates used to compute the averaged value V_{esw} (Fig. 2).

Panel (a) presents the VDF in dependence on $(V_\parallel, V_\perp)$, while panel (b) demonstrates a reduced distribution function computed as $\int \mathrm{VDF}(V_\parallel, V_\perp) 2\pi V_\perp dV_\perp$. The ion VDF consists of at least two beamlike populations, which is typical of the Earth's plasma sheet [34,35]. The reduced ion VDF can be fairly well fitted to beam and core Maxwell populations. The ion core population with temperature of 1.7 keV constitutes about 75% of the total ion density, while the ion beam with temperature around 0.5 keV and velocity around −1120 km/s constitutes about 18% of the total ion density. The other 7% of the ion density is contributed by the wings of the reduced ion VDF, not described by the core and beam populations. The best fit ion parameters indicated in panel (b) are typical of the entire interval. The electron VDF is relatively well described by a drifting Maxwell distribution with temperature of 475 eV, drift velocity smaller than one percent of the electron thermal velocity and density consistent with the total ion density of about 1.25 cm^{-3} within a few percent (Supplemental Material [27]). It is noteworthy that the electron population is several times colder than the ion core population in the entire interval.

Figure 4 shows that a double-humped reduced ion VDF is persistent through the entire interval. The ion beam propagates antiparallel to the local magnetic field, that is in the same direction as the solitary waves. Panel (b) presents temporal evolution of velocities of the local maximum (ion beam) and local minimum of the reduced ion VDF. Intriguingly, the superimposed velocities of the electron holes are closely clustered around local minimums of the ion distribution functions. Panel (c) strengthens that point by demonstrating that the electron hole velocities are correlated with the velocity of the local minimum and not correlated with the ion beam velocity. Importantly, the considered electron holes are not exceptional. We inspected more than 1000 slow electron holes collected in several other intervals in the Earth's plasma sheet. The results of the statistical analysis are presented in the Supplemental Material [27]. We found that, as for the interval presented in detail here, slow electron holes are associated with double-humped ion distribution functions and have velocities around the local minimums of these ion distribution functions. Thus, MMS observations show that slow electron holes in the plasma sheet are very strongly correlated with the presence of a double-humped ion distribution function.

In simulations, electron holes started with zero velocity relative to a Maxwellian ion distribution are observed to accelerate up to speeds greatly exceeding the ion thermal velocity [11–13]. This self-acceleration is attributed to repulsion of the electron hole from a developing depression in the ion density. The theoretical challenge is therefore to understand how slow electron holes can persist with velocities comparable to the bulk of the ion VDF. New theory has recently shown that they *cannot unless* the ion VDF is double humped and their velocity lies within the local minimum of the ion distribution [25]. The effect of this strongly nonthermal ion distribution is to reverse the sign of the ion density perturbation caused by the positive potential, so that the electron hole is no longer repelled but attracted by the ion perturbation it causes.

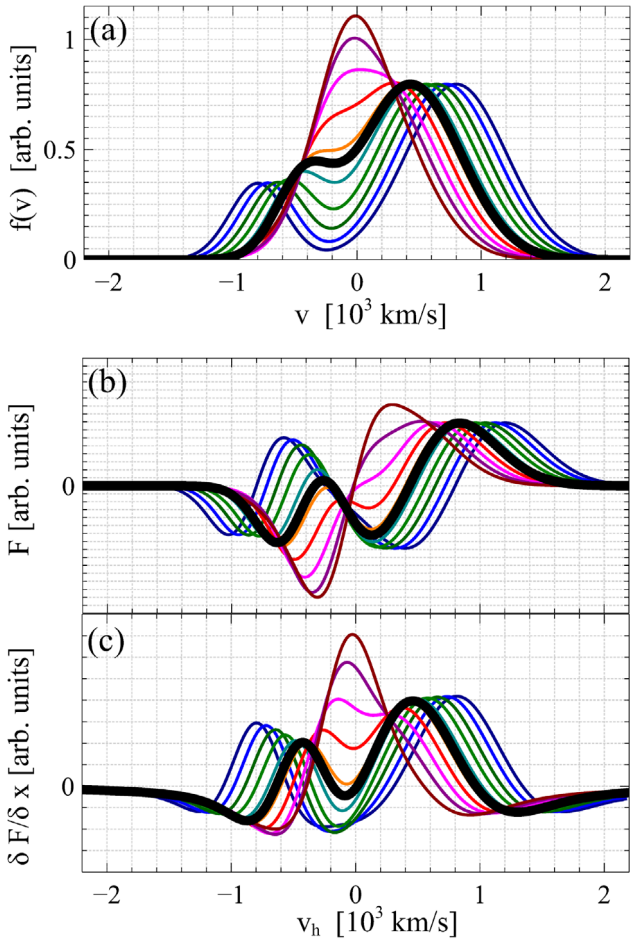

FIG. 5. Results of velocity stability calculations for a slow electron hole typical of the presented interval (amplitude of 10 V and spatial scale of 3 km). The electron hole velocity v_h is a free parameter in the calculations. Panel (a) presents ion distribution functions (in scaled units) consisting of two Maxwellian beams with temperatures and relative densities equivalent to those observed by MMS [Fig. 3(b)], but with various velocity separations between the ion beams. Using recent theory [25], for each ion distribution function we computed force F acting on the electron hole and variation of this force $\delta F/\delta x$ (scaled units), when the electron hole is shifted by δx with respect to the ion density perturbation that it causes. Panels (b) and (c) show the computed F and $\delta F/\delta x$ depending on electron hole velocity v_h. The stable electron hole propagation is possible if and only if $F = 0$ and $\delta F/\delta x < 0$. Bold black line in panel (a) is the ion distribution function marginally stable for the electron hole self-acceleration, while corresponding F and $\delta F/\delta x$ depending on v_h are shown by black solid lines in panels (b) and (c). Ion distributions with this deep a local minimum or deeper are stable, shallower are unstable to self-acceleration of the electron hole.

The stabilizing effect of the local ion distribution minimum has been analyzed quantitatively for a wide range of distribution shapes [25]. The approach is to suppose that the ion density perturbation caused by the electron hole potential is unchanged by the self-acceleration instability, because the ion timescale is relatively long. The electron hole-accelerating force can therefore be calculated for any potential shape shifted laterally by δx relative to the ion density it would cause. If this force δF is such as to enhance the shift, $\delta F/\delta x > 0$, self-acceleration occurs. Otherwise, it does not and a slow electron hole can persist. Note that one must also determine the equilibrium velocity at which the total force F is zero.

Figure 5 presents results of velocity stability calculations for a slow electron hole typical of the considered interval. We assumed a slow electron hole with amplitude of 10 V and spatial scale of 3 km, though specific values of these parameters do not affect the results presented below, when they are in the ranges found in the observations. The one-dimensional ion distribution $f(v)$ is represented by two Maxwellian beams whose temperatures and relative densities coincide with those of the observed reduced ion VDF [Fig. 3(b)]. The free parameters in the calculations are velocity separation between the ion beams and electron hole velocity v_h. For convenience, theoretical analysis was done in the reference frame, where velocities of the two ion beams are equal and opposite. Panel (a) presents ion distribution functions corresponding to various ion beam separations. For each of these ion distributions we computed force F and $\delta F/\delta x$ depending on electron hole velocity v_h. The results of the calculations in panels (b) and (c) show that stable electron hole propagation, $F = 0$ and $\delta F/\delta x < 0$, is possible for ion beam separations exceeding about 800 km/s and only for electron holes with velocities around the local minimums. The marginal distribution to achieve stable electron hole propagation and avoid self-acceleration is refined by iteration and indicated in panel (a). Distributions with this deep a local minimum or deeper are stable, shallower are unstable to self-acceleration of the electron hole. For the observed reduced ion VDF in Fig. 3(b) the separation between the ion beams exceeds 900 km/s and, hence, a local minimum is deep enough to satisfy stability of electron holes with velocities around the local minimum.

In conclusion, electron holes propagating with velocities much larger than ion thermal velocity have previously been widely observed in laboratory experiments [36,37] and various regions of near-Earth space [38–42]. On the contrary, *slow* electron holes have only recently been unambiguously identified in space plasma, and the very existence of these solitary waves has been theoretically puzzling. In this Letter we have presented multisatellite Magnetospheric Multiscale observations showing slow electron holes have velocities lying in the local minimum of double-humped ion velocity distribution functions. Theoretical analysis shows that, whatever is the origin of these structures, this configuration is necessary for the electron holes to remain slow by avoiding the self-acceleration caused by interaction with ions. Note that detailed kinetic calculations show that the plasma in the presented interval is linearly stable to electrostatic waves of ion-acoustic and Buneman type, because electrons are much colder than ions. Therefore, the origin of the slow electron holes still remains a puzzle.

The work of S. K. and A. A. was supported by the Russian Science Foundation Grant No. 19-12-00313. The work of I. V. was supported by NASA Heliophysics Supporting Research Grant No. 80NSSC20K1325 and National Science Foundation Grant No. 2026680. I. V. also thanks for support the International Space Science Institute (ISSI), Bern, Switzerland. We thank the MMS teams for the excellent data publicly [43].

*Serjesmail@gmail.com

[1] I. B. Bernstein, J. M. Greene, and M. D. Kruskal, Exact nonlinear plasma oscillations, Phys. Rev. **108**, 546 (1957).
[2] H. Schamel, Electron holes, ion holes and double layers. Electrostatic phase space structures in theory and experiment, Phys. Rep. **140**, 161 (1986).
[3] Y. Omura, H. Matsumoto, T. Miyake, and H. Kojima, Electron beam instabilities as generation mechanism of electrostatic solitary waves in the magnetotail, J. Geophys. Res. **101**, 2685 (1996).
[4] M. V. Goldman, D. L. Newman, and A. Mangeney, Theory of Weak Bipolar Fields and Electron Holes with Applications to Space Plasmas, Phys. Rev. Lett. **99**, 145002 (2007).
[5] I. H. Hutchinson, Electron holes in phase space: What they are and why they matter, Phys. Plasmas **24**, 055601 (2017).
[6] Y. V. Khotyaintsev, A. Vaivads, M. André, M. Fujimoto, A. Retinò, and C. J. Owen, Observations of Slow Electron Holes at a Magnetic Reconnection Site, Phys. Rev. Lett. **105**, 165002 (2010).
[7] D. B. Graham, Y. V. Khotyaintsev, A. Vaivads, and M. André, Electrostatic solitary waves with distinct speeds associated with asymmetric reconnection, Geophys. Res. Lett. **42**, 215 (2015).
[8] C. Norgren, M. André, A. Vaivads, and Y. V. Khotyaintsev, Slow electron phase space holes: Magnetotail observations, Geophys. Res. Lett. **42**, 1654 (2015).
[9] A. Lotekar, I. Y. Vasko, F. S. Mozer, I. Hutchinson, A. V. Artemyev, S. D. Bale, J. W. Bonnell, R. Ergun, B. Giles, Y. V. Khotyaintsev, P. A. Lindqvist, C. T. Russell, and R. Strangeway, Multisatellite MMS analysis of electron holes in the Earth's Magnetotail: Origin, properties, velocity gap, and transverse instability, J. Geophys. Res. (Space Phys.) **125**, e28066 (2020).
[10] I. Y. Vasko, R. Wang, F. S. Mozer, S. D. Bale, and A. V. Artemyev, On the nature and origin of bipolar electrostatic structures in the earth's bow shock, Front. Phys. **8**, 156 (2020).

[11] B. Eliasson and P. K. Shukla, Dynamics of Electron Holes in an Electron Oxygen-Ion Plasma, Phys. Rev. Lett. **93**, 045001 (2004).
[12] B. Eliasson and P. K. Shukla, Formation and dynamics of coherent structures involving phase-space vortices in plasmas, Phys. Rep. **422**, 225 (2006).
[13] C. Zhou and I. H. Hutchinson, Plasma electron hole kinematics. II. Hole tracking Particle-In-Cell simulation, Phys. Plasmas **23**, 082102 (2016).
[14] L. B. Wilson, III, C. Cattell, P. J. Kellogg, K. Goetz, K. Kersten, L. Hanson, R. MacGregor, and J. C. Kasper, Waves in Interplanetary Shocks: A Wind/WAVES Study, Phys. Rev. Lett. **99**, 041101 (2007).
[15] R. Wang, I. Y. Vasko, F. S. Mozer, S. D. Bale, I. V. Kuzichev, A. V. Artemyev, K. Steinvall, R. Ergun, B. Giles, Y. Khotyaintsev, P. A. Lindqvist, C. T. Russell, and R. Strangeway, Electrostatic solitary waves in the Earth's bow shock: Nature, properties, lifetimes, and origin, J. Geophys. Res. (Space Phys.) **126**, e29357 (2021).
[16] R. E. Ergun, C. W. Carlson, J. P. McFadden, F. S. Mozer, L. Muschietti, I. Roth, and R. J. Strangeway, Debye-Scale Plasma Structures Associated with Magnetic-Field-Aligned Electric Fields, Phys. Rev. Lett. **81**, 826 (1998).
[17] K. G. McClements, M. E. Dieckmann, A. Ynnerman, S. C. Chapman, and R. O. Dendy, Surfatron and Stochastic Acceleration of Electrons at Supernova Remnant Shocks, Phys. Rev. Lett. **87**, 255002 (2001).
[18] M. Hoshino and N. Shimada, Nonthermal electrons at high mach number shocks: Electron shock surfing acceleration, Astrophys. J. **572**, 880 (2002).
[19] H. Che, J. F. Drake, M. Swisdak, and P. H. Yoon, Electron holes and heating in the reconnection dissipation region, Geophys. Res. Lett. **37**, L11105 (2010).
[20] J. F. Drake, M. Swisdak, C. Cattell, M. A. Shay, B. N. Rogers, and A. Zeiler, Formation of electron holes and particle energization during magnetic reconnection, Science **299**, 873 (2003).
[21] J. Büchner and N. Elkina, Anomalous resistivity of current-driven isothermal plasmas due to phase space structuring, Phys. Plasmas **13**, 082304 (2006).
[22] L. P. Dyrud and M. M. Oppenheim, Electron holes, ion waves, and anomalous resistivity in space plasmas, J. Geophys. Res. (Space Phys.) **111**, A01302 (2006).
[23] P. Petkaki, M. P. Freeman, T. Kirk, C. E. J. Watt, and R. B. Horne, Anomalous resistivity and the nonlinear evolution of the ion-acoustic instability, J. Geophys. Res. (Space Phys.) **111**, A01205 (2006).
[24] H. Che, J. F. Drake, M. Swisdak, and P. H. Yoon, Nonlinear Development of Streaming Instabilities in Strongly Magnetized Plasma, Phys. Rev. Lett. **102**, 145004 (2009).
[25] I. H. Hutchinson, How can slow plasma electron holes exist?, Phys. Rev. E **104**, 015208 (2021).
[26] J. L. Burch, T. E. Moore, R. B. Torbert, and B. L. Giles, Magnetospheric multiscale overview and science objectives, Space Sci. Rev. **199**, 5 (2016).
[27] See Supplemental Material at http://link.aps.org/supplemental/10.1103/PhysRevLett.127.165101 for figures supporting several statements in the Letter and results of a statistical analysis of ion velocity distribution functions corresponding to slow electron holes observed by Magnetospheric Multiscale spacecraft in other intervals in the Earth's plasma sheet.
[28] D. J. Gershman, L. A. Avanov, S. A. Boardsen, J. C. Dorelli, U. Gliese, A. C. Barrie, C. Schiff, W. R. Paterson, R. B. Torbert, B. L. Giles, and C. J. Pollock, Spacecraft and instrument photoelectrons measured by the dual electron spectrometers on MMS, J. Geophys. Res. (Space Phys.) **122**, 11548 (2017).
[29] C. T. Russell *et al.*, The magnetospheric multiscale magnetometers, Space Sci. Rev. **199**, 189 (2016).
[30] C. Pollock *et al.*, Fast plasma investigation for magnetospheric multiscale, Space Sci. Rev. **199**, 331 (2016).
[31] R. E. Ergun *et al.*, The axial double probe and fields signal processing for the MMS mission, Space Sci. Rev. **199**, 167 (2016).
[32] P. A. Lindqvist *et al.*, The spin-plane double probe electric field instrument for MMS, Space Sci. Rev. **199**, 137 (2016).
[33] H. Washimi and T. Taniuti, Propagation of Ion-Acoustic Solitary Waves of Small Amplitude, Phys. Rev. Lett. **17**, 996 (1966).
[34] T. E. Eastman, L. A. Frank, W. K. Peterson, and W. Lennartsson, The plasma sheet boundary layer, J. Geophys. Res. **89**, 1553 (1984).
[35] J. Birn, M. Hesse, A. Runov, and X. Z. Zhou, Ion beams in the plasma sheet boundary layer, J. Geophys. Res. (Space Phys.) **120**, 7522 (2015).
[36] W. Fox, M. Porkolab, J. Egedal, N. Katz, and A. Le, Laboratory Observation of Electron Phase-Space Holes during Magnetic Reconnection, Phys. Rev. Lett. **101**, 255003 (2008).
[37] B. Lefebvre, L.-J. Chen, W. Gekelman, P. Kintner, J. Pickett, P. Pribyl, S. Vincena, F. Chiang, and J. Judy, Laboratory Measurements of Electrostatic Solitary Structures Generated by Beam Injection, Phys. Rev. Lett. **105**, 115001 (2010).
[38] R. E. Ergun, C. W. Carlson, J. P. McFadden, F. S. Mozer, L. Muschietti, I. Roth, and R. J. Strangeway, Debye-Scale Plasma Structures Associated with Magnetic-Field-Aligned Electric Fields, Phys. Rev. Lett. **81**, 826 (1998).
[39] C. Cattell, J. Dombeck, J. Wygant, J. F. Drake, M. Swisdak, M. L. Goldstein, W. Keith, A. Fazakerley, M. André, E. Lucek, and A. Balogh, Cluster observations of electron holes in association with magnetotail reconnection and comparison to simulations, J. Geophys. Res. (Space Phys.) **110**, A01211 (2005).
[40] J. R. Franz, P. M. Kintner, J. S. Pickett, and L.-J. Chen, Properties of small-amplitude electron phase-space holes observed by polar, J. Geophys. Res. (Space Phys.) **110**, A09212 (2005).
[41] D. M. Malaspina, L. Andersson, R. E. Ergun, J. R. Wygant, J. W. Bonnell, C. Kletzing, G. D. Reeves, R. M. Skoug, and B. A. Larsen, Nonlinear electric field structures in the inner magnetosphere, Geophys. Res. Lett. **41**, 5693 (2014).
[42] F. S. Mozer, O. V. Agapitov, B. Giles, and I. Vasko, Direct Observation of Electron Distributions inside Millisecond Duration Electron Holes, Phys. Rev. Lett. **121**, 135102 (2018).
[43] https://lasp.colorado.edu/mms/sdc/public/.